Chapter

Pectins as Emulsifying Agent on the Preparation, Characterization, and Photocatalysis of Nano-$LaCrO_3$

Rudy Tahan Mangapul Situmeang

Abstract

The use of environmentally friendly chemicals as the emulsifying agent in the preparation of the advanced materials is a focus and is very interesting to do. Although the focus is important, the advanced material that is made remains a top priority regarding characterization and its activity. One of the chemicals for making advanced and environmentally friendly materials such as $LaCrO_3$ perovskite is pectin functioning as the emulsifying agent. In general, perovskite compounds are materials with very wide applications such as fuel cells, electronic equipment, sensors, magnetic materials, photoluminescent materials, thermic catalysts, and photocatalysts. Furthermore, the use of various solvents to produce perovskite compounds with the aim of getting good applications has been done a lot such as water, alcohols, or other organic solvents, respectively, in mixing precursors directly, precipitation and coprecipitation, microwave, auto-combustion, sol-gel, and hydrothermal methods. In this chapter, preparation of $LaCrO_3$ using pectin as an emulsifying agent will be discussed in advance together with characterization and application of $LaCrO_3$ in the photocatalytic reaction of dyes and cellulose conversion.

Keywords: nanoperovskite, pectin, photocatalysis, dyes, cellulose

1. Introduction

1.1 General introduction of pectin

Pectin is a natural organic compound that has unique structure and characteristics. The uniqueness of the pectin structure is seen from its constituents consisting of three components [1–4], namely, homogalacturonan (HG), rhamnogalacturonan-I (RGI), and rhamnogalacturonan-II (RGII). In principle, the main structure is RG. Furthermore, the functional groups possessed by pectin are ferulic acid, methoxy, acetyl esters, and esters. Interactions between the functional groups that are held provide uniqueness to the characteristics of pectin through hydrogen bonds, hydrophobic interactions, polyelectrolyte behavior, specific ion interactions, and even covalent bonds [5, 6] as external cation binding matrices prepared in the preparation of the advanced material.

Schematically the binding and distribution of cations dissolved in the pectin solution can be illustrated as in **Figure 1**.

In general, pectin can bind various cations with oxidation numbers of +1, +2, and +3 through various functional groups that belong to one or more pectin molecules, so that the cations bound are ready to react to produce a compound that will be well-distributed and the size of the particles produced can reach the nanoscale.

1.2 General introduction of $LaCrO_3$

Perovskite compounds, ABO_3 (where A = cation of alkali, alkaline earth, or lanthanide metal and B = cation of transition metal), have unique chemical and physical properties such as oxidative, magnetic, conductive, refractive, luminescent, and catalytic. With such interesting and valuable characteristics, these compounds have been utilized tremendously in electronic devices as a tuner of the dielectric/ferroelectric responses [7] and an overcomer inefficiency on photovoltaics and other optoelectronic devices [8], sensors as a hydrazine detector [9] and ozone sensing property [10], magnetisms as a huge magnetoresistance [11] and a magnetoelectric response [12], photoluminescences as a highly photoluminescent thin film [13] and a light-emitting material [14], catalysts as CO2/H2 converter into alcohol [15] and pollutant decomposer [16], solid oxide fuel cells as a self-anode in the next power generator [17] and a good performance cathode [18], and photocatalysts as a photo-oxidator of benzylic alcohol [19] and a decomposer of dyes [20].

Perovskite structural material (ABO_3) can be synthesized by mixing the oxide of lanthanide or third main group elements with the oxide of the transition elements. The cations can fit into both the A and B sites of the perovskite structure. In principle, the ABO_3 structure should obey the formulae of Goldschmidt's tolerance factor [21], $t = 0.71(r_A + r_O)/(r_B + r_O)$. This t-value led to the formation of crystalline structures such as cubic [22], orthorhombic [23], and hexagonal forms [24].

One of the perovskite materials, lanthanum chromites ($LaCrO_3$), has been extensively examined due to its applicability as interconnector for solid oxide fuel cell [25], excellent chemical stabilizer [26], good electrical properties at high temperature [27], total oxidation catalyst [28], partial oxidation catalyst [29], oxidative dehydrogenation catalyst [30], and photocatalyst [31]. Nowadays, various kinds of methods have been utilized to prepare the perovskite compounds such as hydrothermal [32, 33], precipitation [34, 35], coprecipitation [36, 37], auto-combustion [38, 39], and sol-gel [40–42]. Among these various kinds of the preparation methods, sol-gel holds particular importance, since it offers many advantages over the others. In the sol-gel technique, a homogeneous product is affected by all steps of preparation such as selection and dissolution of raw material, homogeneous mixing, and pH and temperature adjustments. In addition, these steps led to the opportunity to gain the nanomaterial. Therefore, unique

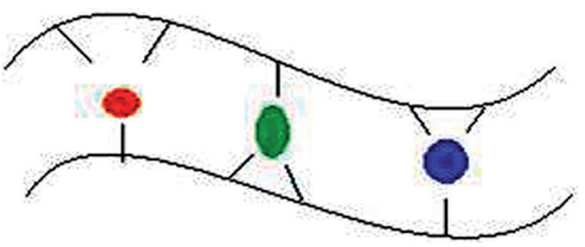

Figure 1.
Illustration of binding of cations by pectin during the dissolution process.

physical and chemical properties of nanomaterial will be more feasible to obtain compared to their micro- and macro-size counterparts in a huge range of updated technologies [43–45].

Since the transformation of raw materials from the dissolved state into a solid state is also crucial in the sol-gel method, gelation, as well as solidification, determines the particle size of the product. To gain the nanomaterial, the agglomeration should be avoided by controlling carefully the process of both gelation and solidification as well as that of thermal treatment.

1.3 Typical property of photocatalyst

In heterogeneous photocatalytic processes, the semiconductors used are chalcogenide-type semiconductor materials (oxides, TiO_2, ZnO, ZrO, and CeO_2, or sulfides, ZnS and CdS). Semiconductors can be used as photocatalyst because they have a void energy region called band-gap energy, which lies between the conduction band boundary (LUMO) and the valence band (HOMO) that does not provide energy for promoting recombination of electrons and holes produced by a photoactivation in these semiconductors.

This semiconductor will function as a catalyst if it is illuminated with photons that have energy that is equal to or more than the energy bandgap (E_g) of the semiconductor used ($h\nu \geq E_g$). Induction by these rays will excite the electrons (from the valence to the conduction band) in semiconductor materials [46]. As a result of the photon illumination, the formation of electron pairs (e^-) and holes (h^+) which are separated into free photoelectrons in the conduction band and photo hole in the valence band is ready to trigger the reaction as shown in **Figure 2**.

The reaction that occurs in this event is:

$$\text{Semiconductor} + h\upsilon \rightarrow \left(e_{CB}^{-} + h_{VB}^{+}\right)$$

There are several possibilities that occur in electron-hole pairs, namely:

1. Some pairs recombine in particles (volume recombination).

2. Electron-hole pairs recombine on the surface (surface recombination) or in bulk particles in just a few nanoseconds (energy is lost as heat).

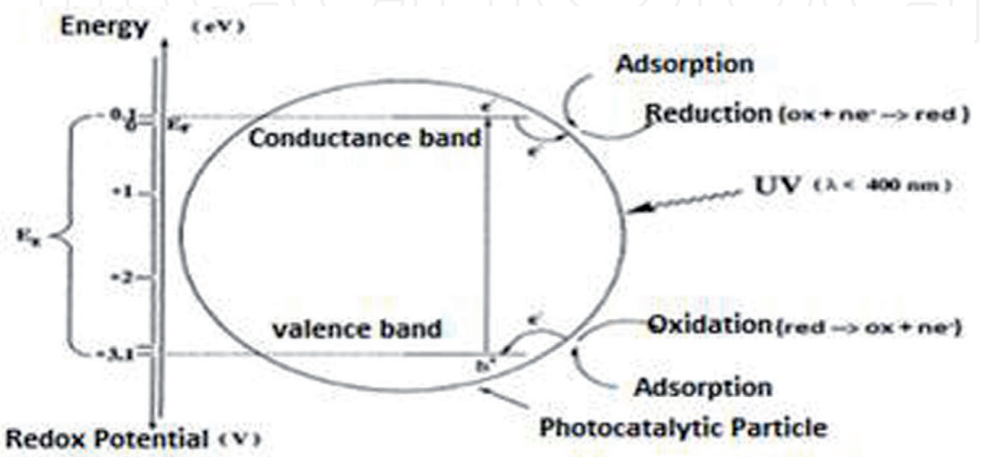

Figure 2.
Band-gap energy diagram in the photocatalytic process ([47]

The electron-hole pair recombination reaction can be written as follows:

$$\text{Semiconductor}\left(e^{-}_{CB} + h^{+}_{VB}\right) \rightarrow \text{semiconductor} + \text{heat}$$

3. Each electron pair can react with donor species (D) and acceptor (A), which are adsorbed on the particle surface. In other words, the electrons in the conduction band that reach the surface will reduce the substrate (A) or solvent on the surface of the particles, while the holes in the valence band will oxidize the substrate (D) either directly or indirectly through hydroxyl radical formation. This phenomenon follows the reaction equation as follows:

$$h\upsilon + \text{semiconductor} \rightarrow e^{-} + h^{+}$$

$$A_{(ads)} + e^{-} \rightarrow A^{-}_{(ads)}$$

$$D_{(ads)} + h^{+} \rightarrow D^{+}_{(ads)}$$

Some possible reactions that can occur with radical ions formed (A^{-} and D^{+}) include:

a. A^{-} and D^{+} react between fellow radical ions or react with adsorbates (species adsorbed to the surface).

b. A^{-} and D^{+} combine by transferring the electron back to form an excited state from one of the reactants or releasing heat.

c. A^{-} and D^{+} diffuse from the surface of the semiconductor and participate in chemical reactions that occur in the solution medium.

In general, the process of the occurrence of a photocatalytic reaction based on the energy-gap concept indicates the difference in HOMO energy (the top band of valence contains electrons) and LUMO (the lowest band of conduction without electrons) that must be passed. In other words, the promotion of electrons from the top band of valence to the lowest band of conduction requires minimum energy equivalent to its band-gap energies. If the energy owned is zero or larger than 4 eV, owned are zero or large (>4 eV), then each is a metal or insulator, whereas semiconductor has energy between these values. Furthermore, the band-gap energy is classified as direct and indirect. Direct means that the minimum energy from the lowest band of conduction is just above the maximum energy of the valence band at the same momentum of crystals. If the condition is not so, it is called indirect band-gap energy. The range of band-gap energy possessed by a material will determine the type of energy that will be used so that a photocatalytic reaction can occur. The type of energy can be used for the reaction as shown in **Figure 3**.

In principle, all light electromagnetic waves can be used as an energy source for a chemical reaction process. So far, light that can be used as a trigger for chemical reactions through electron transfer from the HOMO to the LUMO level in the degradation and/or breaking of a compound bond into an environmentally friendly product is visible and ultraviolet.

Visible radiation is often used to degrade toxic compounds of dyes since the waste of dyes which is channeled directly into a river or sea body will have a negative effect

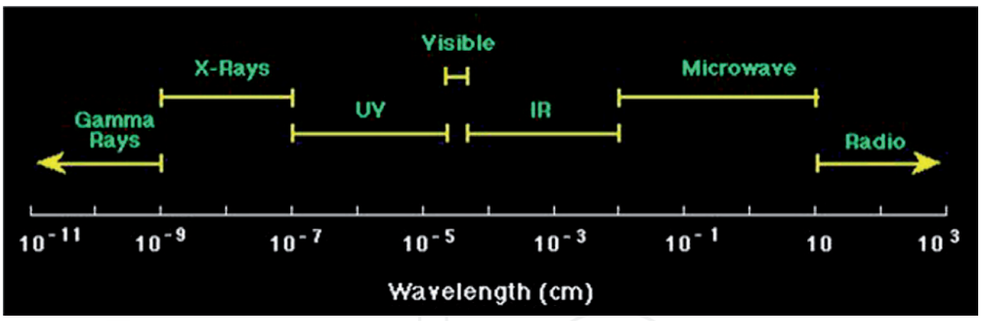

Figure 3.
Schematic radiation energy of electromagnetic wavelength.

Num	Type of bond	Bond energy	
		(kJ/mol)	(eV)
1	H—H	436	11.58
2	C—H	413	10.97
3	O—H	366	9.72
4	C—O	360	9.56
5	C—C	348	9.25
6	C = C	614	16.31
7	C = O	745	19.79
8	C = N	615	16.33
9	C≡C	839	22.29
10	N≡N	941	24.99

Table 1.
Some typical bonds and bond energies.

on aquatic biota. In general, visible light radiation has a wavelength range of 400—800 nm. In other words, the energy needed to break the chemical bonds of a compound is low. Generally, these dyes are compounds that have chromophore groups, such as methine, nitro, azo, anthraquinone, triarylmethane, and phthalocyanine groups. In fact, dyes used in industry can be either natural compounds or syntheses.

Ultraviolet radiation has a high ability to breakdown the bond and cause decomposition because of its high energy compared to infrared radiation and visible light [48]. Sources of ultraviolet radiation can be obtained from sunlight or artificial light. Ultraviolet (UV) radiation of the sun is electromagnetic energy with wavelengths between 200 and 400 nm and has more energy than visible light. Based on its wavelength, solar UV radiation is divided into:

1. UVA with a wavelength of 320—400 nm is a high wavelength and emits radiation of constant magnitude throughout the year. This radiation can cause premature aging of the skin.

2. UVB with a wavelength of 280–320 nm is a shorter wavelength and is more intense than UVA. UVB is more strongly absorbed by several biomolecular pollutants.

3. UVC with a wavelength of 200—280 nm is the most intensive and dangerous UV radiation and has the potential to cause damage to organisms.

Therefore, to choose a type of UV light in photocatalytic reaction depends on the type of bond and the energy required. In general, the type of bond with its energy can be seen in **Table 1**.

2. Method of preparation

Preparation of $LaCrO_3$ catalyst material was carried out using the sol-gel method with pectin as an emulsifying agent. The preparation was conducted by dissolving specified mass of $La(NO_3)_3.9H_2O$ and $Cr(NO_3)_3.6H_2O$, respectively, in 100 mL of pectin solution (4 g pectin). The overall procedure was described in the previous article [49].

3. Characterizations

Before the material made was applied, the photocatalyst was characterized to determine the physical and chemical properties associated through X-ray diffraction analysis, electron transmission microscopy, distribution of particle distribution, energy-gap, and functional groups related to the structural formation and the acidity of Brønsted-Lowry and Lewis.

3.1 Analysis of X-ray diffraction

X-ray diffraction can be utilized to identify the phase formed and the relative percentages of different phases of the materials obtained. Then, the real structural parameters like particle size, lattice parameters (a, b, and c), lattice volume, and theoretical density can be calculated from their diffractogram using Rietveld calculation [50].

X-ray diffraction experiments are carried out by the procedure as described in the previous article [49]. To know the crystallite size, the representative peak of a diffractogram can be elucidated by using the Scherrer method of calculation [51]. The results of the diffractogram, determination of the size of the crystalline phase, and the Rietveld calculation are presented in **Figure 4**.

In general, the results of $LaCrO_3$ prepared using pectin provide a single crystalline phase, nanosize, and other parameter values shown in **Table 2**.

3.2 Transmission electron microscope analysis

TEM can be used to study the morphology and surface characteristics of the perovskite nanomaterials. To evaluate the surface morphology, the samples were

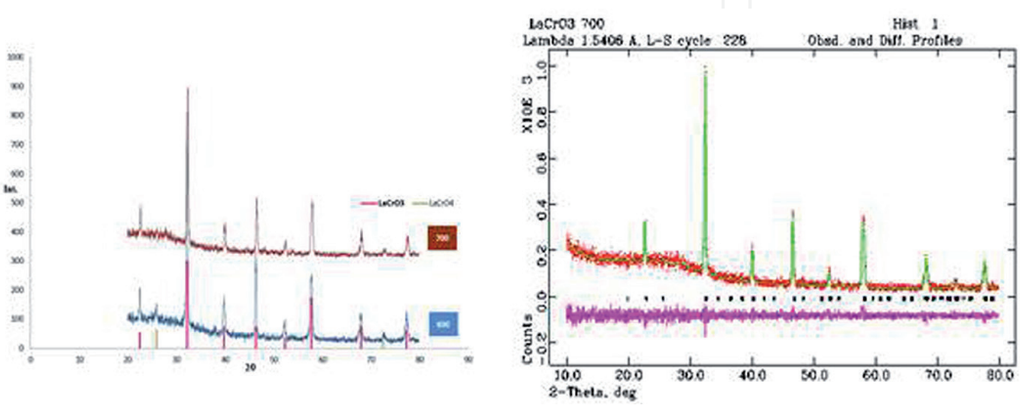

Figure 4.
Diffractogram of $LaCrO_3$ (a) experimental results and (b) the result of the Rietveld calculation using $LaCrO_3$ calcined at 700°C.

Num	Parameter	$LaCrO_3$ calcined at			Ref
		600°C	700°C	800°C	
1	Crystalline phase	Cubic	Orthorhombic	Orthorhombic	[50]
2	Crystalline size (nm)	24.84	24.12	27.09	[48]
3	hkl plane	110	112	121	[50]

Table 2.
Parameters of $LaCrO_3$ prepared in various calcination temperatures.

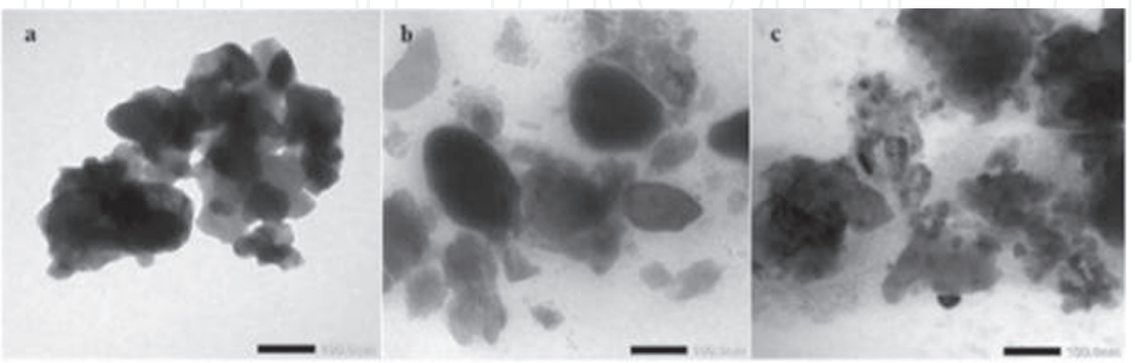

Figure 5.
TEM micrographs of $LaCrO_3$ prepared using pectin as the emulsifying agent: calcined at (a) 600, (b) 700, and (c) 800°C.

characterized using TEM. The analysis was conducted on polished and thermally etched samples with different magnifications. TEM results of $LaCrO_3$ material are presented in **Figure 5**.

It seems that there is still a relatively large region of agglomeration in the crystalline phase formed in each of these preparations. Nevertheless, the particle sizes obtained using TEM in this study are significantly smaller than that of $LaCrO_3$ prepared using sol-gel method reported by another research group [52]. It was found that the particle sizes of the sample calcined at 600, 700, and 800°C are 34.6, 30, and 28 nm, respectively.

3.3 Particle size distribution analysis

Analysis of the particle size distribution of the solid sample was examined by the technique of dynamic light scattering (DLS). The measurement of the sample using this instrument can be determined by either wet or dry method. If a measurement is using the wet method, the sample is prepared using alcohol dispersant such as methanol, ethanol, or propanol. However, if the measurement is using a dry method on preparing the sample, air dispersant could be utilized. More information can be obtained in the manual book [53]. The more important in preparing sample is to prevent the irreversible change to the particle (dissolution, milling, or aggregation) happened.

From **Figure 6**, it can be implied that there are two or three regions of the particle size which are quantum dot, nano-, and micron sizes. Overall, it can be said that nanosize of the particles 21.9, 86.4, and 89.11% referred to $LaCrO_3$ calcined at 600, 700, and 800°C, respectively [49].

The results also can be implied that the more nanosize particle obtained, the higher the temperature of calcination applied. In other words, the temperature of calcination plays a role to determine the nanosize of the particle. In other studies,

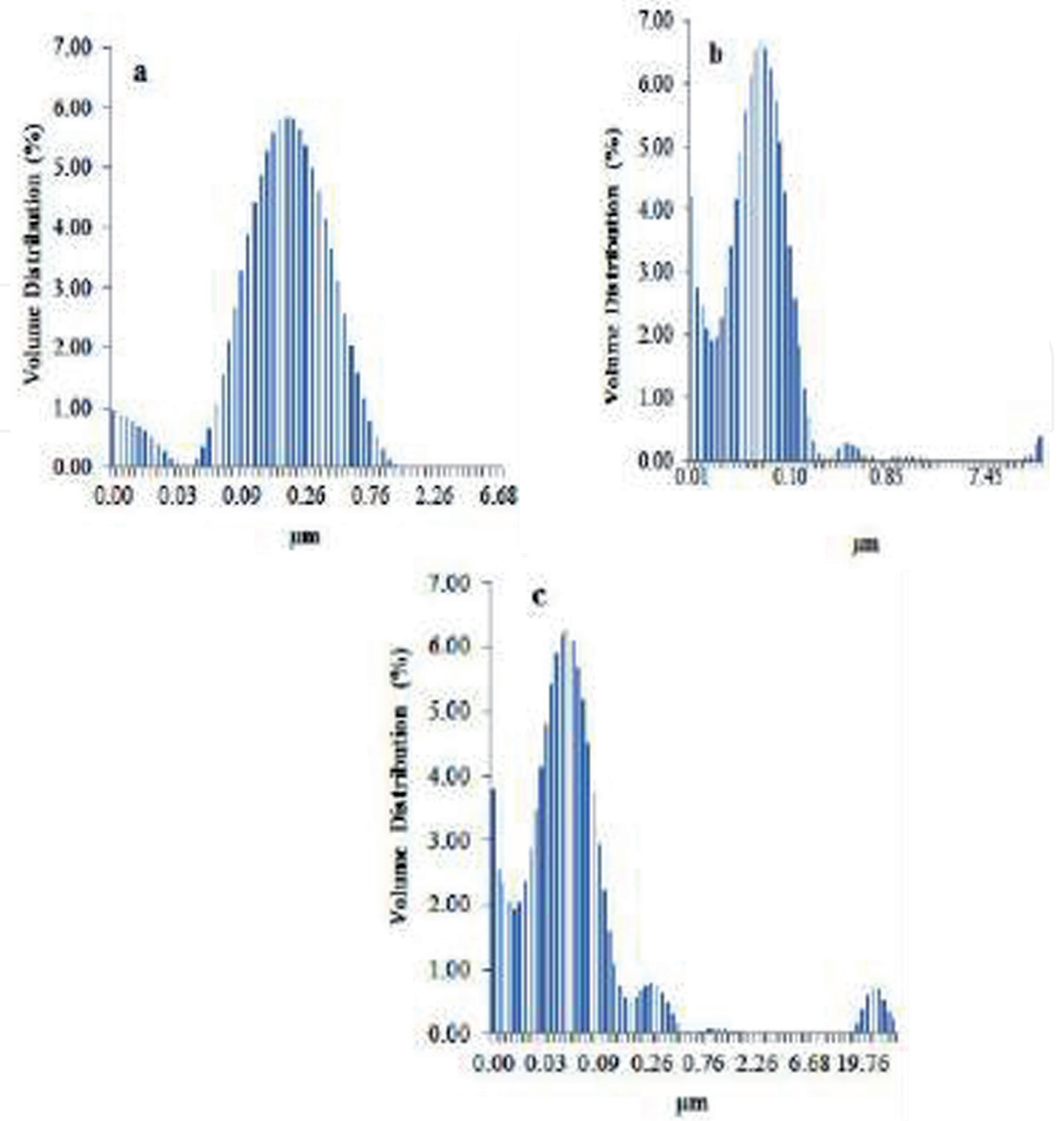

Figure 6.
The particle size distribution of the $LaCrO_3$ calcined at (a) 600, (b) 700, and (c) 800°C.

the particle size of $LaCrO_3$ prepared using hydrothermal method was determined by PSA method. The result proved that the average size of particle is in the range of micron [54] and 57 nm [55].

3.4 Analysis of diffuse reflectance UV-Vis spectroscopy

In order to know the band-gap energy of the $LaCrO_3$ prepared in a different calcined temperature, the analysis was run using diffuse reflectance UV-Vis spectroscopy as shown in **Figure 7**.

To determine the bandgap of a powder sample using the diffuse reflectance spectrophotometer is a common technique [56]. So, in this study the band-gap energy is calculated using a Kubelka-Munk method [57] based on the equation below:

$$\alpha(h\nu) \approx \beta \left(h\nu - E_{op}\right)^{n}$$

where β is a constant and n is an index related to the possible type of electron transition. The value of n could be 1/2, 2, 3/2, and 3. Those values are corresponding

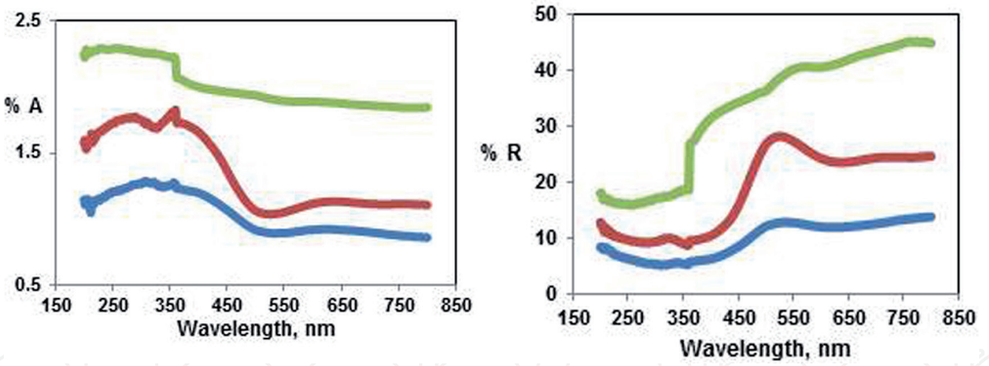

Figure 7.
Reflectance (A) and absorption (B) features of $LaCrO_3$ calcined at 600, 700, and 800°C, respectively.

to the nature of electron transition. In principle, there are two kinds of electron transition, which are direct and indirect. If the n value is 1/2 or 2, it means allowed direct or indirect electron transition happened. But if the n value is 3/2 or 3, it means forbidden direct or indirect electron transition occurred [58].

The results of the band-gap energy from $LaCrO_3$ calcined at 600, 700, and 800°C, respectively, are 2.62, 2.89, and 2.98 eV. The magnitude of those band-gap energies is suitable for photocatalytic reactions using UV and visible light irradiation.

3.5 Fourier transform infrared analysis

In principle, FTIR analysis in the material field is used to assess the functional groups and what bonds are formed in the material prepared in relation to the expected compound. In preparing samples for their analysis, the procedures performed are standard and can be referenced in various libraries [49, 59, 60].

The chemical bonding and chemical structure of the prepared perovskites can be identified. The FTIR spectra can give structural confirmation supporting XRD analysis. Infrared spectra of $LaCrO_3$ material are presented in **Figure 8**.

From **Figure 8**, it can be implied that perovskite $LaCrO_3$ is actually formed and can be assessed based on the type of bond vibration which can be referred to in detail in the following literature [a]. The La—O—La and La—O—Cr bonds through

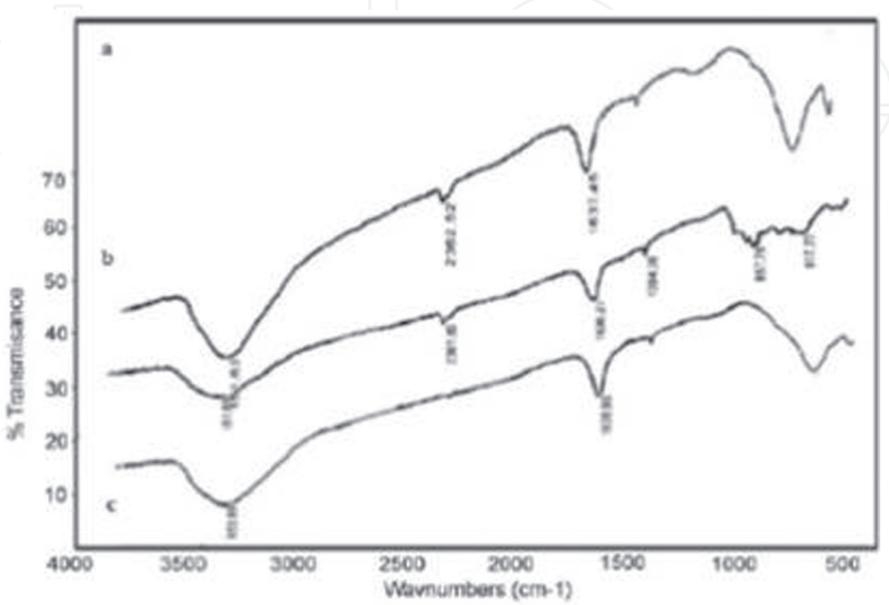

Figure 8.
Infrared spectra of $LaCrO_3$ calcined at (a) 600°C, (b) 700°C, and (c) 800°C [48].

information on bending vibrations are increasingly apparent as the calcination temperature increases. In other words, the structure of $LaCrO_3$ which is formed along with the increase in the calcination temperature is getting closer and can be assessed through the diffractogram data.

The results also reflect that the existence of Brønsted-Lowry and Lewis acid sites is indicated by the presence of absorption bands at wave number 1400 and 1630 cm^{-1}, respectively. In detail, the acidity characteristics of the $LaCrO_3$ calcined at the various temperatures were described in the previous article [49].

4. Applications

The advanced material $LaCrO_3$ prepared using pectin emulsifier and then tested on dye degradation and cellulose conversion was described below.

4.1 Photocatalysis of dye

The photocatalytic activity test on $LaCrO_3$ nanocatalysts was carried out on the methanyl yellow compound by mixing as much as 0.08 g of $LaCrO_3$ nanocatalyst into 300 mL methanyl yellow with a concentration of 100 ppm into a beaker and then homogenized. After that the mixture was pipetted as much as 20 mL with various time variations (0, 10, 20, 30, 40, and 50 min) which had been irradiated by a UV lamp with a distance of 30 cm. After that, UV-Vis spectrophotometry was tested to see the absorbance rate of methanyl yellow.

Then in the photocatalytic reaction for visible light, as much as 0.08 g of $LaCrO_3$ catalyst was put into 300 mL of 100 ppm methanyl yellow in a beaker. Then homogenized it by stirring, while the sample is placed that the mixture is placed under the sun in the range of time 11 am to 1 pm. Then the sample was pipetted as much as 20 mL with various time variations (0, 10, 20, 30, 40, and 50 min) and tested with UV-Vis spectrophotometry to see the absorbance rate of methanyl yellow. Photodegradation under UV light irradiation is shown in **Figure 9**.

4.2 Photocatalysis of cellulose

The application of $LaCrO_3$ photocatalyst to cellulose conversion was carried out on a laboratory scale using procedural as follows:

The $LaCrO_3$ catalyst was then used in the photocatalytic test process for the conversion of nanocellulose to sugar alcohol. As much as 0.5 g of nanocellulose in 100 mL of distilled water are distilled for 30 min. The nanocellulose solution that has been ultrasonified is transferred into a three-neck flask, then stirred with

(a) (b)

Figure 9.
Dye photodegradation results under visible light irradiation (a) and ultraviolet (b) for 0–50 min.

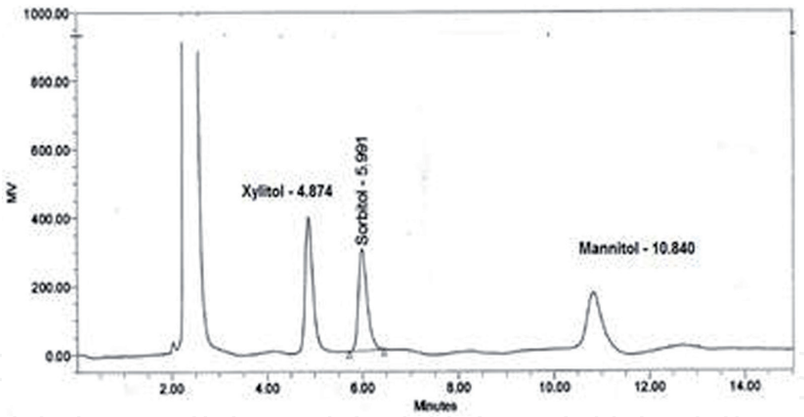

Figure 10.
Photocatalytic cellulose conversion results using $LaCrO_3$ under ultraviolet light irradiation during 1 h exposure.

a stirrer, and then added $LaCrO_3$ nanocatalyst as much as 0.1 g. Furthermore, hydrogen gas is flowed and irradiated with UV light with a variation of time 15, 30, 45, and 60 min. The reaction results were analyzed by high-performance liquid chromatography (HPLC). The results of photocatalytic cellulose conversion using $LaCrO_3$ under UV light are shown in **Figure 10**.

Quantitatively, the results obtained are compared with the standard results for each xylitol sorbitol solution, and the concentration of mannitol is known. Then the quantitative results of the experiment, even though it is still relatively small, are, respectively, 190, 180, and 120 ppm at 1 h exposure with UV radiation [61].

5. Conclusions

Preparation of advanced materials using the sol-gel method with pectin emulsifier is able to make the active catalyst degrade methanyl yellow dyes and convert cellulose into glucose reducing sugars and sugar alcohols such as xylitol, sorbitol, and mannitol. The particle size and crystalline produced by the preparation method can reach nanosize with a range of 24-50 nm. Furthermore, the band-gap energy results state that the $LaCrO_3$ advanced material is in the range of 2.89–3.0 eV.

Acknowledgements

The author would like to acknowledge both the financial support from Indonesian Government through the Directorate Research, Ministry of Research and Higher Education on the contract number 384/UN26.21/PN/2018 in doing the Research and the Research Institution and Community services of the University of Lampung for funding this book chapter.

Author details

Rudy Tahan Mangapul Situmeang
Department of Chemistry, Faculty of Mathematics and Natural Sciences, University of Lampung, Lampung, Indonesia

*Address all correspondence to: rudy.tahan@fmipa.unila.ac.id

References

[1] Willats WG, McCartney L, Mackie W, Knox JP. Pectin: Cell biology and prospects for functional analysis. Plant Molecular Biology. 2001;**47**(1-2):9-27

[2] O'Neill MA, Ishii T, Albersheim P, Darvill AG. Rhamnogalacturonan II: Structure and function of a borate cross-linked cell wall pectic polysaccharide. Annual Review of Plant Biology. 2004;**55**:109-139

[3] Schols HA, Voragen AGJ. Complex pectins: Structure elucidation using enzymes. Progress in Biotechnology. 1996;**14**:3-19

[4] Voragen AGJ, Coenen GJ, Verhoef RP, Schols HA. Pectin, a versatile polysaccharide present in plant cell walls. Structural Chemistry. 2009;**20**:263

[5] Daas PJH, Meyer Hansen K, Schols HA, De Ruiter GA, Voragen AGJ. Investigation of the non-esterified galacturonic acid distribution in pectin with endo-polygalacturonase. Carbohydrate Research. 1999;**318**:135-145

[6] Braccini I, Grasso R, Perez S. Conformational and configurational features of acidic polysaccharides and their interactions with calcium ions: A molecular modeling investigation. Carbohydrate Research. 1999, 1999;**317**(1-4):119-130

[7] Li B-W, Osada M, Kim Y-H, Ebina Y, Akatsuka K, Sasaki T. Atomic layer engineering of high-κ ferroelectricity in 2D perovskites. Journal of the American Chemical Society. 2017;**139**:10868-10874

[8] Tsai H, Asadpour R, Blancon J-C, Stoumpos CC, Ajayan PM, Nie W, et al. Design principles for electronic charge transport in solution-processed vertically stacked 2D perovskite quantum wells. Nature Communications. 2018;**9**:2130

[9] Ali SM, Al Lehaibi HA. Smart perovskite sensors: The electrocatalytic activity of SrPdO for hydrazine oxidation. Journal of The Electrochemical Society. 2018;**165**(9):B345-B350

[10] Kakavelakis G, Petromichelaki V, Gagaoudakis E, Binas V, Kiriakidis G, Petridis K, et al. Solution processed $CH_3NH_3PbI_{3-x}Cl$ perovskite based self-powered ozone sensing element operated at room temperature. ACS Sensors. 2018;**3**:135-142

[11] Borchani SM, Koubaa WC-R, Megdiche M. Structural, magnetic and electrical properties of a new double-perovskite $LaNaMnMoO_6$ material. Royal Society Open Science. 2017;**4**:170920

[12] Casallas F, Vera E, Landinez D, Parra C, Roa J. Structural properties, electric response and magnetic behaviour of $La_2SrFe_2CoO_9$ triple complex perovskite. Journal of Physics Conference Series. 2016;**687**:012047

[13] González-Carrero S, Martínez-Sarti L, Sessolo M, Galian RE, Pérez-Prieto J. Highly photoluminescent, dense solid films from organic-capped $CH_3NH_3PbBr_3$ perovskite colloids. Journal of Physical Chemistry C. 2018;**6**:6771-6777

[14] Lao X, Yang Z, Su Z, Wang Z, Ye H, Wang M, et al. Luminescence and thermal behaviors of free and trapped excitons in cesium lead halide perovskite nanosheets. Nanoscale. 2018;**10**:9949-9956

[15] Situmeang R, Supriyanto R, Septanto M, Simanjuntak W, Sembiring S, Roger AC. $Ni_xCo_yFe_{1-x-y}O_4$ nanocatalyst:

Preparation, characterization, and acitvity in CO_2/H_2 conversion. Proceedings of the 2nd International Conference Indonesian Chemical Society. (October 22-23th, Universitas Islam Indonesia, Yogyakarta) 2013:103-110

[16] Patel F, Patel S. $La_{1-x}Sr_xCoO_3$ (x=0, 0.2) perovskites type catalyst for carbon monoxide emission control from auto-exhaust. Process Engineering. 2013;**51**:324-329

[17] Sengodan S, Ishihara T, Ju Y-W, Shin J, Kwon O, Kim G. Self-decorated MnO nanoparticles on double perovskite solid oxide fuel cell anode by in situ exsolution. ACS Sustainable Chemistry & Engineering. 2017;**5**:9207-9213

[18] Jun A, Kim J, Shin J, Kim G. Perovskite as a cathode material: A review of its role in solid-oxide fuel cell technology. ChemElectroChem. 2016;**3**:511-530

[19] Huang H, Yuan H, Janssen KPF, Solís-Fernández G, Wang Y, Collin Y, et al. Efficient and selective photocatalytic oxidation of benzylic alcohols with hybrid organic-inorganic perovskite materials. ACS Energy Letters. 2018;**3**(4):755-759

[20] Kong J, Yang T, Rui Z, Ji H. Perovskite-based photocatalysts for organic contaminants removal: Current status and future perspectives. Catalysis Today. 2018. DOI: 10.1016/j.cattod.2018.06.045

[21] Goldschmidt VM. Die Gesetze der krystallochimie. Die Naturwissenschaften. 1926;(21):477-485

[22] Wang S, Wu X, Yuan L, Zhang C, Cui X, Lu D. Hydrothermal synthesis, morphology, structure and magnetic properties of perovskite structure $LaCr_{1-x}Mn_xO_3$ (x=0.1, 0.2 and 0.3). CrystEngComm. 2018. DOI: 10.1039/C8CE00421H

[23] Chen Y, Qin H, Shi C, Li L, Hu. High temperature CO2 sensing properties and mechanism of nanocrystalline $LaCrO_3$ with rhombohedral structure: Experiments and ab initio calculations. RSC Advances. 2015;**5**:54710

[24] Coşkun M, Polat O, Coşkun FM, Durmus Z, Çaglar M, Türüt A. The electrical modulus and other dielectric properties by the impedance spectroscopy of $LaCrO_3$ and $LaCr_{0.90}Ir_{0.10}O_3$ perovskites. RSC Advances. 2018;**8**:4634

[25] Kumar Y, Regalado-Pérez E, Ayala AM, Mathews NR, Mathew X. Effect of heat treatment on the electrical properties of perovskite solar cells. Solar Energy Materials & Solar Cells. 2016;**157**:10-17

[26] Rao Y, Wang Z, Chen L, Wu R, Peng R, Lu Y. Structural, electrical, and electrochemical properties of cobalt doped $NiFe_2O_4$ as a potential cathode material for solid oxide fuel cells. International Journal of Hydrogen Energy. 2013;**38**(4):14329

[27] Tiwari B, Dixit A, Naik R, Lawes G, Rao MSR. Dielectric and optical phonon anomalies near antiferromagnetic ordering in $LaCrO_3$: A possible near room temperature magnetodielectric system. Applied Physics Letters. 2013;**103**:152906

[28] Zhang Z, Kong Z, Liu H, Chen Y. Frontiers of Chemical Science and Engineering. 2014;**8**(1):87-94

[29] Khine MSS, Chen L, Zhang S, Lin J, Jiang SP. International Journal of Hydrogen Energy. 2013;**38**:13300-13308

[30] Dinse A, Frank B, Hess C, Habel D, Schomäcker R. Journal of Molecular Catalysis A: Chemical. 2008;**289**:28-37

[31] Kanhere P, Chen Z. Mole. 2014;**19**:19995-20022

[32] Kang M, Yun J, Cho C, Kim C, Tai W. Open Journal of Inorganic Non-metallic Materials. 2013;**3**:37-42

[33] Rivas-Vázquez LP, Rendón-Angeles JC, Rodríguez-Galicia JL, Gutiérrez-Chavarria CA, Zhu KJ, Yanagisawa K. Journal of the European Ceramic Society. 2006;**26**(1-2):81-88

[34] Chettapongsaphan C, Charojrochkul S, Assabumrungrat S, Laosiripojana N. Asian Journal of Energy and Environment. 2008;**9**(1-2):101-119

[35] Doggali P, Grasset F, Cador O, Rayalu S, Teraoka Y, Labhsetwar N. Journal of Environmental Chemical Engineering. 2014;**2**:340

[36] Kumar S, Teraoka Y, Joshi AG, Rayalu S, Labhsetwar N. Journal of Molecular Catalysis A: Chemical. 2011;**348**:42

[37] Yanping W, Junwu Z, Xiaojie S, Xujie Y. Journal of Rare Earths. 2007;**25**:601-610

[38] Corrêa HPS, Paiva-Santos CO, Setz LF, Martinez LG, Mello-Castanho SRH, Orlando MTD. Powder Diffraction. 2008;**23**(2):S18-S22

[39] Tong Y, Ma J, Zhao S, Huo H, Zhang H. Journal of Nanomaterials. 2015;**115**:1-5

[40] Doggali P, Rayalu S, Teraoka Y, Labhsetwar N. Journal of Environmental Chemical Engineering. 2015;**3**:420

[41] Meng M, Guo X, Dai F, Li Q, Zhang Z, Jiang Z, et al. Applied Catalysis B: Environmental. 2013;**142-143**:278-289

[42] Situmeang R, Manurung P, Sulistiyo ST, Hadi S, Simanjuntak W, Sembiring S. Asian Journal of Chemistry. 2015;**27**(3):1138-1142

[43] Girish H-N, Shao GQ , Basavalingu B. RSC Advances. 2016;**6**:79763-79767

[44] Chen W, Chen X, Yang Y, Yuan J, Shangguan W. International Journal of Hydrogen Energy. 2014;**39**:13468-13473

[45] López-Suárez FE, Bueno-López A, Illán-Gómez MJ, Trawczynski J. Applied Catalysis A: General. 2014;**485**:214-221

[46] Richardson JT. Principles of Catalyst Development. New York: Plenum Press; 1989. xv, 288 pp., ISBN 0-306-43162-9

[47] Herrmann J-M. Heterogeneous photocatalysis: Fundamentals and applications to the removal of various types of aqueous pollutants. Catalysis Today. 1999;**53**:115-129

[48] Ibhadon AO, Fitzpatrick P. Heterogeneous photocatalysis: Recent advances and applications. Catalysts. 2013;**3**(1):189-218

[49] Situmeang R, Supryanto R, Kahar LNA, Simanjuntak W, Sembiring S. Characteristics of nanosize $LaCrO_3$ prepared through sol-gel route using pectin as emulsifying agent. Oriental Journal of Chemistry. 2017;**33**(4):1705-1713

[50] Rietveld HM. A profile refinement method for nuclear and magnetic structures. Journal of Applied Crystallography. 1969;**2**:65-71

[51] Cullity BD, Stock SR. Elements of X-Ray Diffraction. 3rd ed. Prentice-Hall Inc.; 2001. pp. 167-171. ISBN 0-201-61091-4

[52] Rativa-Parada W, Gomez-Cuaspud JA, Vera-Lopez E, Carda JB. Structural and electrical study of $LaCrO_3$ modifiedwith Fe and Co. Journal of Physics: Conference Series. 2017;**786**:012029

[53] Rawle A. A Basic Guide to Particle Characterization. Malaysia: Malvern Instrument Limited; 2012. pp. 1-8

[54] Sardar K, Lees Martin R, Kashtiban RJ, Sloan J, Walton Richard I. Direct hydrothermal synthesis and physical properties of rare-earth and yttrium orthochromite perovskites. Chemistry of Materials. 2011;**23**:48-56

[55] Athawale AA, Desai PA. Silver doped lanthanum chromites by microwave combustion method. Ceramics International. 2011;**137**:3037-3043

[56] López R, Gómez R. Band-gap energy estimation from diffuse reflectance measurements on sol–gel and commercial TiO_2: A comparative study. Journal of Sol-Gel Science and Technology. 2012;**61**:1-7

[57] Sangiorgi N, Aversa L, Tatti R, Verucchi R, Sanson A. Spectrophotometric method for optical band gap and electronic transitions determination of semiconductor materials. Optical Materials. 2017;**64**:18-25

[58] Urbach F. The long-wavelength edge of photographic sensitivity and of the electronic absorption of solids. Physical Review. 1953;**92**(5):1324

[59] Yazýcý DT, Bilgiç C. Determining the surface acidic properties of solid catalysts by amine titration using Hammett indicators and FTIR-pyridine adsorption methods. Surface and Interface Analysis. 2010;**42**(6):959-962

[60] ASTM 4824-13. Test method for determination of catalyst acidity by pyridine chemisorption. MNL 58-EB. 2013

[61] Situmeang R, Sembiring Z, Simarmata E, Tamba M, Yuliarni T, Simanjuntak W, Sembiring S. Advances in Natural Sciences: Nanoscience and Nanotechnology. 2019;**10**(1):0150xx